

Environment-Aware Network-Level Design of Generalized Pinching-Antenna Systems—Part I: Traffic-Aware Case

Yanqing Xu, *Senior Member, IEEE*, Zhiguo Ding, *Fellow, IEEE*, Xiu Yin Zhang, *Fellow, IEEE*, Trung Q. Duong, *Fellow, IEEE*, and Tsung-Hui Chang, *Fellow, IEEE*

Abstract—Existing studies on generalized pinching-antenna systems are predominantly link-level, which optimize system parameters for a given user set with objectives defined by per-user performance metrics. Such designs do not directly capture network-level requirements, e.g., region-wide coverage and location fairness, and may require frequent re-optimization as users move or enter/leave, incurring control overhead and sensitivity to localization errors. Motivated by this gap, this two-part paper aims to develop an environment-aware network-level design framework for generalized pinching-antenna systems. Part I focuses on the traffic-aware case, where user presence is modeled statistically by a spatial traffic map and performance is optimized and evaluated in a traffic-aware sense; Part II addresses the geometry-aware case in obstacle-rich environments by explicitly modeling line-of-sight blocking and optimizing region-wide robustness objectives. In Part I, we introduce traffic-weighted average signal-to-noise ratio (SNR) metrics and formulate two traffic-aware deployment problems: (i) maximizing the traffic-weighted network average SNR, and (ii) a fairness-oriented traffic-restricted max-min average-SNR design over traffic-dominant grids. To solve these nonconvex problems with low complexity, we reveal and exploit their separable structures. For the network-average objective, we establish unimodality properties of the hotspot-induced components and develop a candidate-based global maximization method that only needs to evaluate the objective at a small set of candidate antenna positions. For the traffic-restricted max-min objective, we develop a block coordinate decent framework where each coordinate update reduces to a globally solvable one-dimensional subproblem via an epigraph reformulation and bisection. Simulations show that traffic-aware pinching-antenna positioning consistently outperforms representative fixed and heuristic traffic-aware deployments in the considered setups.

Index Terms—Generalized pinching antenna, environment-aware design, traffic-weighted optimization, traffic-restricted optimization.

I. INTRODUCTION

Wireless systems are increasingly assessed by area-wide service quality rather than the peak rate of a single scheduled

Y. Xu is with the School of Science and Engineering, The Chinese University of Hong Kong, Shenzhen, 518172, China (email: xuyanqing@cuhk.edu.cn).

Z. Ding is with the School of Electrical & Electronic Engineering, Nanyang Technological University, 639798, Singapore (e-mail: zhiguo.ding@ntu.edu.sg).

X. Y. Zhang is with the School of Microelectronics, South China University of Technology, Guangzhou 510000, China, and also with the Pazhou Laboratory, Guangzhou 510330, China (e-mail: eexyz@scut.edu.cn).

T. Q. Duong is with the Faculty of Engineering and Applied Science, Memorial University, St. John's, NL A1C 5S7, Canada and also with the School of Electronics, Electrical Engineering and Computer Science, Queen's University Belfast, Belfast, U.K. (e-mail: tduong@mun.ca).

T.-H. Chang is with the School of Artificial Intelligence, The Chinese University of Hong Kong, Shenzhen, 518172, China (email: changtsunghui@cuhk.edu.cn).

link. In practice, operators must provide reliable and fair coverage over an entire service region, especially in deployments where both user demand and propagation conditions vary remarkably across space. User presence is often non-uniform and clustered around traffic hotspots [1], while blockage, scattering, and irregular layouts create location-dependent channels with LoS corridors and shadowed zones [2], [3]. Consequently, network performance is jointly governed by the spatial traffic distribution and geometry-induced propagation characteristics. This motivates a shift from link-level tuning to network-level optimization grounded in spatial statistics, where performance is evaluated over a discretized region using metrics such as (traffic-weighted) spatially averaged signal-to-noise ratio (SNR), SNR-threshold coverage probability, and worst-location robustness.

Conventional network-level optimization typically tunes configuration parameters of a fixed infrastructure, e.g., antenna tilts/beam patterns, transmit powers, and cell-level control knobs, to improve region-wide coverage and capacity. A representative example is the self-organizing-network line of work on coverage-and-capacity optimization, where remote electrical tilts and power settings are adapted based on network measurements (e.g., call traces) to address overshooting and coverage holes while balancing spectral efficiency; related formulations also optimize antenna tilts via utility/fairness criteria at the network level [4], [5]. In parallel, map-based paradigms such as radio environment maps (REM) and channel-knowledge maps (CKMs) advocate learning location-tagged propagation statistics to enable environment-aware resource management across grids [6]. However, CKM-centric designs primarily capture propagation knowledge and do not explicitly encode where/when users appear and demand concentrates; as emphasized by the perception-embedding-map framework (PEMNet), network optimization fundamentally benefits from jointly embedding channel and fine-grained spatial-temporal traffic knowledge, since traffic maps determine the relevant operating points and bottlenecks that channel maps alone cannot reveal [7]. Recent data-driven “digital-twin” frameworks further aim to support network-level optimization by building measurement-grounded simulators and localized channel/coverage maps so that network behaviors can be evaluated and optimized off-line rather than through costly trial-and-error in live networks [8], [9].

Despite their success, these approaches are fundamentally built on a fixed infrastructure and therefore share an inherent

limitation: the radiating sites remain physically anchored, so optimization can primarily reshape *how* a given site radiates (e.g., via tilt, power, or beam pattern adaptation) but cannot change *where* energy is injected into the environment. Consequently, both environment-induced and demand-induced non-uniformities can persist at the network level. In blockage-rich environments, coverage tails and worst-location performance are often dictated by a small set of severely shadowed or far-corner grids that are difficult to lift through parameter tuning alone. Meanwhile, when user traffic is highly heterogeneous, fixed-site configurations may struggle to deliver sufficient service to shifting hotspots without sacrificing performance elsewhere. These limitations motivate architectures that introduce an additional, structured spatial degree of freedom at the infrastructure level.

Generalized pinching-antenna systems offer precisely such a capability by enabling on-demand signal radiation at selectable locations along an extended guiding medium (e.g., dielectric waveguides or leaky structures) [10], allowing the network to adapt the effective radiation origin to both spatial demand and propagation geometry. Specifically, the radio frequency (RF) signal is guided along a medium and selectively radiated at configurable points, creating short-hop links near users and enabling the coverage “injection points” to be reconfigured after deployment. This expands the design space beyond conventional controls that only reshape how a fixed site radiates (e.g., tilt, power, beamforming), by additionally controlling where energy is injected via repositioning/activating radiating points along the medium. Such spatial actuation is particularly valuable for area-wide objectives, as it can steer coverage toward high-demand regions and mitigate geometry-induced dead zones (e.g., obstacle shadows) by choosing more favorable radiating locations. In this two-part paper, we develop an environment-aware, network-level design framework for generalized pinching-antenna systems that accounts for both demand distribution and propagation geometry, together with low-complexity optimization algorithms to configure radiating points for improved region-wide performance.

In the literature, generalized pinching-antenna systems have received rapidly growing attention due to their unique capability of enabling large-scale spatially reconfigurable transmission by creating configurable radiating points along an extended guiding medium. Considering NTT DOCOMO’s dielectric waveguide-based pinching antenna [11], the work in [12] established fundamental electromagnetic/system models and showcased that pinching antennas can flexibly form strong LoS-dominant links with reduced propagation loss by adjusting the radiation locations. Building on this foundation, the downlink rate maximization problem in a single-waveguide setting was investigated in [13], where a two-stage design was proposed to jointly reduce large-scale attenuation and promote favorable signal combining at the receiver. The study was subsequently extended to multiuser and multi-waveguide regimes in [14]–[17], demonstrating that jointly optimizing the pinching-antenna locations and transmit beamforming can substantially improve spectral and/or energy efficiencies. To further enhance spectral efficiency through user multiplexing, NOMA-enabled pinching-antenna transmission was explored

in [18]–[20], where multiple users’ signals are superposed and conveyed through the same guiding medium. In parallel, the integration of pinching antennas with emerging paradigms such as integrated sensing and communication (ISAC) has been studied in [21]–[23]. By leveraging the capability of pinching antennas to reconfigure LoS links, an environment division multiple access (EDMA) technique was proposed in [24], further highlighting the potential of pinching antennas for multiuser communications. Beyond dielectric-waveguide realizations that are especially attractive at high carrier frequencies, recent work [25] proposed an LCX-based pinching-antenna architecture that enables reconfigurable leakage positions by selectively activating/deactivating radiation slots, thereby turning conventional fixed-leakage LCX into an on-demand radiating structure while retaining the robustness and cost advantages of coaxial cables.

Nevertheless, all existing studies are *link-level* in nature, i.e., they optimize system parameters for a given user set (often assuming accurate user locations or channel state information) with objectives such as per-user SINR/rate. This focus does not directly address *network-level* service requirements that operators care about, such as area-wide coverage, fairness across locations, and robustness under spatially heterogeneous demand and environment-induced shadowing. Moreover, because link-level designs are typically tied to instantaneous user geometry, the optimized pinching locations may need to be recomputed whenever users move or enter/leave the system, which can incur substantial control and computational overhead in high-mobility scenarios; the required reliance on accurate user positioning also makes link-level solutions sensitive to localization errors, leading to non-negligible performance loss when user locations are imperfect. Therefore, improving an average link metric does not necessarily lift the network-level performance. These considerations motivate environment-aware *network-level* design methodologies for generalized pinching-antenna systems, where the objective is defined over a service region based on spatial statistics (e.g., traffic maps and/or geometry maps), enabling designs that are less dependent on instantaneous user positions and more robust to mobility and localization uncertainty.

Motivated by this gap, and without loss of generality focusing on dielectric-waveguide-based pinching antennas as a representative realization, this two-part paper develops an environment-aware network-level design framework for generalized pinching-antenna systems under two complementary settings: the *traffic-aware* case and the *geometry-aware* case. In Part I, we consider traffic-aware network-level optimization, where user presence is characterized statistically by a spatial traffic distribution and performance is evaluated in a traffic-aware sense. Part II complements this study by focusing on geometry-aware design in obstacle-rich environments, where the environment-induced LoS blocking structure is explicitly modeled and area-wide objectives such as coverage and worst-location robustness are optimized. In Part I, the main contributions are summarized as follows:

- **Traffic-aware network-level modeling and metrics:** We develop a tractable traffic-aware network-level framework for pinching-antenna systems by (i) modeling user

presence over the service region via a Gaussian-mixture hotspot traffic map, and (ii) defining a traffic-weighted network average-SNR metric that evaluates long-term coverage quality under random LoS/non LoS (NLoS) fading. To enable efficient optimization, we further introduce a grid-based approximation that discretizes the continuous traffic integral into a numerically tractable weighted sum over representative spatial grids.

- **Traffic-aware problem formulations and optimizations:** Building on the proposed traffic-aware grid model, we formulate two pinching-antenna deployment problems: (i) maximizing the traffic-weighted network average SNR, and (ii) a fairness-oriented traffic-restricted max-min average-SNR design that maximizes the worst average SNR over an active-grid set. To solve these nonconvex problems with low complexity, we exploit their inherent separable structures. Specifically, for the network-average objective, we express each per-waveguide term as a traffic-weighted superposition of hotspot-induced unimodal components, reveal the ensuing merge-split behavior (via a detailed two-hotspot analysis), and develop a candidate-based *global maximization* algorithm that only needs to compare the objective values over a small set of candidate antenna positions. For the traffic-restricted max-min objective, we adopt a block coordinate descent (BCD) framework and show that each coordinate update reduces to a globally solvable one-dimensional subproblem, which can be efficiently handled via bisection on its epigraph form.

Extensive simulations demonstrate that the proposed low-complexity traffic-aware algorithms achieve compelling performance in terms of the considered metrics, and that pinching-antenna systems significantly outperform the fixed-antenna benchmark across a wide range of system settings.

The rest of the paper is organized as follows. Section II presents the system model, the probabilistic LoS/NLoS channel model, and the proposed traffic-aware network-level performance metrics together with their grid-based approximation. Section III formulates the traffic-weighted network average-SNR maximization problem and develops an efficient projected gradient-ascent algorithm. Section IV considers a fairness-oriented traffic-restricted max-min average-SNR design and proposes a low-complexity BCD algorithm with bisection-based coordinate updates. Section V provides numerical results and performance discussions. Finally, Section VI concludes the paper.

II. MODELS AND PERFORMANCE METRICS

In this section, we present the system, channel, and traffic models, as well as the performance metrics and design objectives considered in this work.

A. System Model

Let us first introduce the system model. In this work, we consider a downlink pinching-antenna system where N dielectric waveguides are deployed above a rectangular communication region of size $D_x \times D_y$, as shown in Fig. 1. The waveguides are aligned along the x -axis at a height d_v and

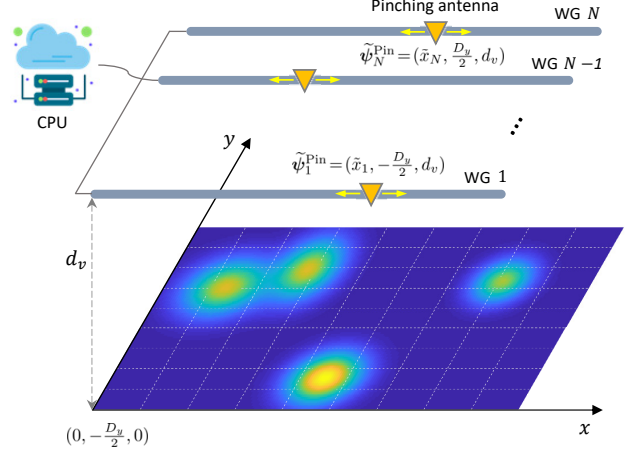


Fig. 1: Traffic-aware pinching-antenna systems.

arranged uniformly in the vertical (y -) direction across the coverage region. Let $\mathcal{N} \triangleq \{1, 2, \dots, N\}$ denote the index set of waveguides. The spacing between adjacent waveguides is denoted by d_h and is chosen as $d_h = \frac{D_y}{N-1} \gg \lambda$, where λ is the carrier wavelength. This ensures that mutual coupling between different waveguides can be neglected. The coordinates of the feed point on the n -th waveguide are $\psi_{0,n} = [0, (n-1)d_h - \frac{D_y}{2}, d_v]^T, \forall n \in \mathcal{N}$. Each waveguide is equipped with a single pinching antenna. The position of the pinching antenna on the n -th waveguide is denoted by $\psi_n^{\text{pin}} = [\tilde{x}_n, \tilde{y}_n, d_v]^T, \tilde{x}_n \in [0, D_x]$ is tunable and $\tilde{y}_n = (n-1)d_h - \frac{D_y}{2}$ is fixed. The pinching antennas' horizontal positions are collected into a vector $\tilde{\mathbf{x}} = [\tilde{x}_1, \dots, \tilde{x}_N]^T$. All waveguides are connected to a common baseband processing unit, which enables coherent joint transmission.

In this work, we focus on the downlink SNR experienced by a typical scheduled user. In each time-frequency resource, at most one user is served, and the BS transmits one data symbol s with $\mathbb{E}[|s|^2] = 1$ across all N pinching antennas with total power P . For a user located at position $\psi = [x, y, 0]^T, 0 \leq x \leq D_x, -\frac{D_y}{2} \leq y \leq \frac{D_y}{2}$, let $\mathbf{h}(\psi, \tilde{\mathbf{x}}) = [h_1(\psi, \tilde{\mathbf{x}}), \dots, h_N(\psi, \tilde{\mathbf{x}})]^T$ denote the vector of complex baseband channel coefficients from the N pinching antennas to this user.

The received signal is given by

$$\mathbf{y} = \sqrt{P} \mathbf{h}^T(\psi, \tilde{\mathbf{x}}) \mathbf{w} s + n, \quad (1)$$

where $\mathbf{w} \in \mathbb{C}^N$ is the beamforming vector, and $n \sim \mathcal{CN}(0, \sigma^2)$ denotes additive white Gaussian noise (AWGN), with $\mathcal{CN}(0, \sigma^2)$ denoting the circularly symmetric complex Gaussian distribution with zero mean and variance σ^2 . Under single-user operation, the BS applies maximum-ratio transmission (MRT) and the MRT beamformer is given by

$$\mathbf{w} = \frac{\mathbf{h}^*(\psi, \tilde{\mathbf{x}})}{\|\mathbf{h}(\psi, \tilde{\mathbf{x}})\|_2}, \quad \|\mathbf{w}\|^2 = 1, \quad (2)$$

which is optimal in terms of SNR for a single scheduled user under a sum-power constraint. Therefore, the corresponding instantaneous SNR at position ψ is given by

$$\Gamma(\psi, \tilde{\mathbf{x}}) = \frac{P}{\sigma^2} \|\mathbf{h}(\psi, \tilde{\mathbf{x}})\|_2^2 \triangleq \rho \|\mathbf{h}(\psi, \tilde{\mathbf{x}})\|_2^2, \quad (3)$$

where $\rho \triangleq P/\sigma^2$ denotes the transmit SNR.

B. Channel Model with Random LoS and NLoS Components

The wireless channel between the n -th pinching antenna and a user at position $\psi = [x, y, 0]^\top$ is modeled as the superposition of a probabilistic LoS component and a NLoS scattering component [26], which is given by

$$h_n(\psi, \tilde{x}) = \xi_n h_n^{\text{LoS}}(\psi, \tilde{x}) + h_n^{\text{NLoS}}(\psi, \tilde{x}). \quad (4)$$

For a user at $\psi = [x, y, 0]^\top$, the LoS channel component $h_n^{\text{LoS}}(\psi, \tilde{x})$ is given by¹

$$h_n^{\text{LoS}}(\psi, \tilde{x}) = \frac{\sqrt{\eta} e^{-j\left(\frac{2\pi}{\lambda} \sqrt{(x-\tilde{x}_n)^2 + C_n} + \frac{2\pi}{\lambda_g} \tilde{x}_n\right)}}{\sqrt{(x-\tilde{x}_n)^2 + C_n}}, \quad (5)$$

where $C_n = ((n-1)d_h - \frac{D_y}{2})^2 + d_y^2$, λ is the free-space wavelength, λ_g is the guided wavelength in the waveguide, and $\eta = \frac{c^2}{(4\pi f_c)^2}$ is a frequency-dependent constant, with c denoting the speed of light and f_c denoting the carrier frequency. We also define the distance between the n -th pinching antenna and the user as $r_n(\psi, \tilde{x}) \triangleq \sqrt{(x-\tilde{x}_n)^2 + C_n}$.

The Bernoulli random variable $\xi_n \in \{0, 1\}$ indicates the presence ($\xi_n = 1$) or absence ($\xi_n = 0$) of a direct LoS path between the user and the antenna. The probability of a LoS path is a function of the distance $r_n(\psi, \tilde{x})$, which is modeled as

$$\Pr[\xi_n = 1] = p_{\text{LoS}}(r_n(\psi, \tilde{x})) = e^{-\beta r_n^2(\psi, \tilde{x})}, \quad (6)$$

where $\beta \geq 0$ is an environment-dependent parameter that controls the likelihood of a LoS path [29], [30].

The NLoS channel component, $h_n^{\text{NLoS}}(\psi, \tilde{x})$, is modeled by the channel gain as a sum of multipath components from scattered paths. We assume that the NLoS path gain follows a Rayleigh fading model with a random as

$$h_n^{\text{NLoS}}(\psi, \tilde{x}) = \sum_{c=1}^{N_c} g_{n,c}(\psi, \tilde{x}), \quad (7)$$

where N_c is the number of NLoS clusters, and $g_{n,c}(\psi, \tilde{x})$ represents the small-scale fading of the c -th NLoS cluster for the n -th antenna, which is assumed to be a zero-mean complex Gaussian random variable with a user-to-antenna distance-dependent variance

$$g_{n,c}(\psi, \tilde{x}) \sim \mathcal{CN}\left(0, \frac{\mu_{n,c}^2}{r_n^2(\psi, \tilde{x})}\right), \quad (8)$$

where $\mu_{n,c}^2$ represents the average power of the c -th NLoS cluster for the n -th antenna. Assume that the NLoS paths are independent, the NLoS path gain follows $h_n^{\text{NLoS}}(\psi, \tilde{x}) \sim \mathcal{CN}(0, \frac{\mu_n^2}{r_n^2(\psi, \tilde{x})})$, where $\mu_n^2 = \sum_{c=1}^{N_c} \mu_{n,c}^2$.

In this work, we do not focus on the instantaneous SNR of a particular user, but network-level performance metrics, i.e., the average SNR according to where users are likely to

¹For simplicity, we omit the in-waveguide attenuation in the LoS channel model. This choice is motivated by the analytical results in [27], [28], which indicate that ignoring in-waveguide attenuation typically has a limited impact on performance, particularly under probabilistic LoS-blockage conditions.

appear. To this end, we next introduce a traffic-aware spatial user model based on Gaussian hotspots, which characterizes the distribution of active user positions and serves as the basis for the subsequent grid-based approximation and optimization of \tilde{x} .

C. Traffic Model

Let $\mathbf{U} = [X, Y]^\top$ denote the random horizontal position of a typical scheduled user on the plane $z = 0$. We model the probability of user appearance over a region as a mixture of two-dimensional Gaussian “hotspots” [31]. Accordingly, the probability density function (PDF) of \mathbf{U} is

$$f_{\mathbf{U}}(x, y) = \sum_{\ell=1}^L \alpha_\ell \mathcal{N}([x, y]^\top; \boldsymbol{\mu}_\ell, \boldsymbol{\Sigma}_\ell), \quad (9)$$

where L is the number of hotspots, $\alpha_\ell \geq 0$ denotes the traffic intensity (mixture weight) of hotspot ℓ satisfying $\sum_{\ell=1}^L \alpha_\ell = 1$, and $\mathcal{N}(\cdot; \boldsymbol{\mu}_\ell, \boldsymbol{\Sigma}_\ell)$ denotes the Gaussian probability distribution function (PDF) with mean $\boldsymbol{\mu}_\ell$ and covariance $\boldsymbol{\Sigma}_\ell$. Here, $\boldsymbol{\mu}_\ell = [\mu_{\ell,x}, \mu_{\ell,y}]^\top$ specifies the hotspot center on the horizontal plane, i.e., $\mu_{\ell,x}$ and $\mu_{\ell,y}$ are the x - and y -coordinates of hotspot ℓ , respectively. Moreover, we adopt a diagonal covariance model $\boldsymbol{\Sigma}_\ell = \text{diag}(\sigma_{\ell,x}^2, \sigma_{\ell,y}^2)$, where $\sigma_{\ell,x}^2$ and $\sigma_{\ell,y}^2$ characterize the traffic spread (variance) of hotspot ℓ along the x - and y -directions, respectively.

At each scheduling instant, the position of the scheduled user can be regarded as an independent realization of \mathbf{U} . This traffic-aware model captures the fact that users are much more likely to appear around a few dominant hotspots (such as offices, meeting rooms, or production lines), while user density decays away from these centers according to the Gaussian tails.

D. Traffic-Aware Network Performance Metric

In fading environments with probabilistic LoS/NLoS conditions, it is important to evaluate how well a given pinching-antenna deployment matches the spatially non-uniform traffic demand. In this work, we adopt a traffic-aware metric based on the average SNR, which captures the long-term link quality experienced by a typical active user whose location follows the hotspot traffic map.

For a fixed deployment \tilde{x} , the local average SNR at position (x, y) is defined as

$$\bar{\Gamma}(x, y; \tilde{x}) \triangleq \mathbb{E}[\Gamma(\psi, \tilde{x}) \mid \psi = [x, y, 0]^\top], \quad (10)$$

where the expectation is taken over random LoS/NLoS channels for a user fixed at (x, y) .

The traffic map $f_{\mathbf{U}}(x, y)$ specifies how likely an active user is to appear around each position. Accordingly, $\bar{\Gamma}(x, y; \tilde{x}) f_{\mathbf{U}}(x, y)$ represents the traffic-weighted local contribution of position (x, y) to the overall SNR performance, combining the channel quality at (x, y) and the probability that this position is populated.

By averaging this contribution over all possible user positions, we obtain the traffic-aware network average SNR

$$\bar{\Gamma}_{\text{net}}(\tilde{x}) \triangleq \iint \bar{\Gamma}(x, y; \tilde{x}) f_{\mathbf{U}}(x, y) dx dy, \quad (11)$$

which represents the expected SNR experienced by a typical active user whose position is drawn according to the hotspot traffic map. It therefore serves as a traffic-aware measure of coverage quality. In other words, it emphasizes regions where users are more likely to appear and quantifies how effectively the pinching-antenna deployment supports the dominant traffic patterns in the service area.

As seen, directly optimizing (11) is non-trivial, since it involves a two-dimensional integral over $f_{\mathbf{U}}(x, y)$ and an expectation over the hybrid LoS/NLoS channel, neither of which admits a simple closed-form expression in general. This motivates the grid-based approximation introduced in the next subsection, where the service area and traffic distribution are discretized into a finite set of representative grids to enable tractable optimization of $\tilde{\mathbf{x}}$.

E. Grid-Based Approximation

To obtain a tractable network-level formulation, we discretize the rectangular communication region of size $D_x \times D_y$ into N_h grids along the horizontal (x -) direction and N_v grids along the vertical (y -) direction. Let

$$\Delta_u \triangleq \frac{D_x}{N_h}, \quad \Delta_v \triangleq \frac{D_y}{N_v} \quad (12)$$

denote the grid sizes in the horizontal and vertical directions, respectively. The center of grid (u, v) is then given by

$$x_u = \left(u - \frac{1}{2}\right) \Delta_u, \quad y_v = -\frac{D_y}{2} + \left(v - \frac{1}{2}\right) \Delta_v, \quad (13)$$

for $u = 1, \dots, N_h$ and $v = 1, \dots, N_v$. The corresponding representative user position in grid (u, v) on the plane $z = 0$ is $\psi_{u,v} = [x_u, y_v, 0]^\top$.

Using this grid-based approximation, the continuous random position \mathbf{U} is approximated by a discrete random variable that takes values in the finite set of grid centers $\{\psi_{u,v}\}$ with probabilities $\{p_{u,v}\}$. In particular, based on the Gaussian-mixture traffic model in (9), the probability of grid (u, v) can be approximated by

$$p_{u,v} \approx f_{\mathbf{U}}(x_u, y_v) \Delta_u \Delta_v, \quad (14)$$

followed by a normalization such that $\sum_{u=1}^{N_h} \sum_{v=1}^{N_v} p_{u,v} = 1$. In this way, expectations with respect to \mathbf{U} can be approximated by finite weighted sums over the grids.

For a given pinching-antenna deployment $\tilde{\mathbf{x}}$, the instantaneous SNR experienced by a user located in grid (u, v) is approximated by

$$\Gamma_{u,v}(\tilde{\mathbf{x}}) \triangleq \Gamma(\psi_{u,v}, \tilde{\mathbf{x}}), \quad (15)$$

with corresponding average SNR defined as

$$\bar{\Gamma}_{u,v}(\tilde{\mathbf{x}}) \triangleq \mathbb{E}[\Gamma_{u,v}(\tilde{\mathbf{x}})], \quad (16)$$

where the expectation and probability are taken over the LoS/NLoS channels, conditioned on the user being in grid (u, v) .

Under this grid-based approximation, the traffic-aware average-SNR-based metric in (11) is evaluated by

$$\bar{\Gamma}_{\text{net}}(\tilde{\mathbf{x}}) \approx \sum_{u=1}^{N_h} \sum_{v=1}^{N_v} p_{u,v} \bar{\Gamma}_{u,v}(\tilde{\mathbf{x}}), \quad (17)$$

which provide numerically tractable discrete counterparts of the continuous-domain metrics (11). This grid-based expression form the basis for the optimization problems studied in the subsequent sections.

III. TRAFFIC-WEIGHTED AVERAGE-SNR OPTIMIZATION

In this section, we aim to maximize the traffic-weighted network average SNR by optimizing the pinching-antenna positions for the given user traffic distribution. In what follows, based on the grid-based approximation, we first derive closed-form expressions for the per-grid and network average SNR. We then formulate the corresponding optimization problem and develop an efficient algorithm to solve it.

A. Per-Grid and Network Average SNR Derivations

Recall that, under the grid-based model, the communication region is discretized into grids indexed by (u, v) with centers $\psi_{u,v} = [x_u, y_v, 0]^\top$, and the traffic weight of grid (u, v) is $p_{u,v}$. For a given deployment $\tilde{\mathbf{x}}$, the instantaneous SNR experienced by a user located in grid (u, v) is denoted by

$$\Gamma_{u,v}(\tilde{\mathbf{x}}) = \rho \|\mathbf{h}(\psi_{u,v}, \tilde{\mathbf{x}})\|_2^2 = \rho \sum_{n=1}^N |h_n(\psi_{u,v}, \tilde{\mathbf{x}})|^2, \quad (18)$$

where $\mathbf{h}(\psi_{u,v}, \tilde{\mathbf{x}})$ collects the channels from all N pinching antennas to grid (u, v) , and the channels of antennas are independent.

Lemma 1 *For a given pinching-antenna deployment $\tilde{\mathbf{x}}$, the local average SNR in grid (u, v) admits the closed-form expression*

$$\bar{\Gamma}_{u,v}(\tilde{\mathbf{x}}) = \rho \sum_{n=1}^N \frac{\eta \exp(-\beta r_{n,u,v}^2(\tilde{\mathbf{x}}_n)) + \mu_n^2}{r_{n,u,v}^2(\tilde{\mathbf{x}}_n)}, \quad (19)$$

where $r_{n,u,v}(\tilde{\mathbf{x}}) = \sqrt{(x_u - \tilde{x}_n)^2 + C_n}$ denotes the distance between pinching antenna n and grid (u, v) . With the traffic weights $\{p_{u,v}\}$, the corresponding traffic-aware network average SNR is given by

$$\bar{\Gamma}_{\text{net}}(\tilde{\mathbf{x}}) \approx \rho \sum_{u=1}^{N_h} \sum_{v=1}^{N_v} p_{u,v} \sum_{n=1}^N \frac{\eta \exp(-\beta r_{n,u,v}^2(\tilde{\mathbf{x}}_n)) + \mu_n^2}{r_{n,u,v}^2(\tilde{\mathbf{x}}_n)}. \quad (20)$$

Proof: See Appendix A. ■

B. Problem Formulation

Based on (20), the traffic-weighted network average-SNR maximization problem is formulated as

$$\max_{\tilde{\mathbf{x}}} \bar{\Gamma}_{\text{net}}(\tilde{\mathbf{x}}) \quad (21a)$$

$$\text{s.t. } 0 \leq \tilde{x}_n \leq D_x, \quad \forall n \in \mathcal{N}, \quad (21b)$$

where $\tilde{\mathbf{x}} = [\tilde{x}_1, \dots, \tilde{x}_N]^\top$ collects the pinching-antenna positions along the N waveguides.

Problem (21) has a simple box-constrained feasible set and a smooth objective: $\bar{\Gamma}_{\text{net}}(\tilde{\mathbf{x}})$ is continuously differentiable in $\tilde{\mathbf{x}}$ since each per-grid average SNR depends smoothly on

the distances $r_{n,u,v}(\tilde{x}_n)$. However, (21) is generally nonconvex because the average SNR term in (19) involves nonlinear distance-dependent components (e.g., the path-loss factor $1/r_{n,u,v}^2(\tilde{x}_n)$ and the attenuation/LoS-related factor embedded in the numerator), which can lead to multiple stationary points. Despite the nonconvexity of (21), the objective admits a favorable separable structure across pinching antennas, which will be formalized in the following lemma and will be exploited to develop low-complexity algorithms.

Lemma 2 *The traffic-weighted network average SNR in (21) can be decoupled over the pinching antennas as*

$$\bar{\Gamma}_{\text{net}}(\tilde{\mathbf{x}}) = \sum_{n=1}^N f_n(\tilde{x}_n), \quad (22)$$

where the n -th component $f_n(\cdot)$ is given by

$$f_n(\tilde{x}) \triangleq \rho \sum_{u=1}^{N_h} \sum_{v=1}^{N_v} p_{u,v} \frac{\eta \exp(-\beta r_{n,u,v}^2(\tilde{x})) + \mu_n^2}{r_{n,u,v}^2(\tilde{x})}. \quad (23)$$

Proof: Starting from the definition of the traffic-weighted network average SNR and substituting the closed-form per-grid average SNR in (19), we have

$$\begin{aligned} \bar{\Gamma}_{\text{net}}(\tilde{\mathbf{x}}) &= \rho \sum_{u=1}^{N_h} \sum_{v=1}^{N_v} p_{u,v} \sum_{n=1}^N \frac{\eta \exp(-\beta r_{n,u,v}^2(\tilde{x}_n)) + \mu_n^2}{r_{n,u,v}^2(\tilde{x}_n)} \\ &\stackrel{(a)}{=} \sum_{n=1}^N \rho \sum_{u=1}^{N_h} \sum_{v=1}^{N_v} p_{u,v} \frac{\eta \exp(-\beta r_{n,u,v}^2(\tilde{x}_n)) + \mu_n^2}{r_{n,u,v}^2(\tilde{x}_n)} \\ &= \sum_{n=1}^N f_n(\tilde{x}_n), \end{aligned} \quad (24)$$

where step (a) follows by rearranging the finite sums (i.e., interchanging the order of summation over (u, v) and n). The proof is complete. ■

Using Lemma 2 and the separable box constraint set in (21b), problem (21) decomposes into N independent scalar maximization problems:

$$\max_{0 \leq x \leq D_x} f_n(x), \quad \forall n \in \mathcal{N}. \quad (25)$$

Each $f_n(x)$ is continuously differentiable on $[0, D_x]$. Nevertheless, $f_n(x)$ is generally nonconcave and may admit multiple local maximizers, since it is a traffic-weighted superposition of many grid-wise terms that are individually peaked around different horizontal grid centers.

Despite this nonconcavity, (25) is substantially simpler than the original N -dimensional problem (21), as it involves only a single scalar variable with a compact feasible interval. In principle, a globally optimal solution can be obtained by a one-dimensional search over $[0, D_x]$, and the overall optimum of (21) is then obtained by concatenating the N independently optimized coordinates. However, when D_x is large and/or a fine search resolution is required, repeating such searches for all N waveguides may still incur non-negligible complexity. This motivates a dedicated solver that explicitly exploits the one-dimensional structure of (25) while providing a principled way to handle the nonconcavity of $f_n(x)$.

C. Problem Structure Analysis and Low-Complexity Algorithm Design

In this section, we aim to develop low-complexity solution approaches to avoid the prohibitive cost of exhaustive search while preserving global optimality under the adopted objective model. To this end, we start from the separable per-waveguide formulation and further express each per-waveguide objective as a traffic-weighted superposition of hotspot-induced components. We then characterize the key structural properties of each component (e.g., smoothness and unimodality). Building on these properties, we study the two-hotspot case in detail to expose the fundamental merge-split behavior of the superposition, which leads to a candidate-based maximization strategy that attains the global maximizer by comparing only a small number of stationary and boundary candidates. Finally, we extend the same principle to the general multi-hotspot case, yielding scalable algorithms that remain effective as the number of hotspots grows.

To obtain clean structural insights, we work with the continuous-domain definition of the traffic-weighted network average SNR, while the connection to the grid-based implementation will be discussed in Remark 1 at the end of this subsection.

Recall that, under the fully random-channel model adopted in this paper, the traffic-weighted network average SNR can be written in a separable form as

$$\bar{\Gamma}_{\text{net}}(\tilde{\mathbf{x}}) = \sum_{n=1}^N \iint_{\mathcal{D}} \bar{\Gamma}_n(x, y; \tilde{x}_n) f_{\mathbf{U}}(x, y) dx dy, \quad (26)$$

where $f_{\mathbf{U}}(x, y)$ is the spatial traffic density over the service region $\mathcal{D} \subset \mathbb{R}^2$ given in (9), and $\bar{\Gamma}_n(x, y; \tilde{x}_n)$ denotes the average SNR at location $(x, y, 0)$ contributed by waveguide n when its pinching antenna is placed at horizontal coordinate \tilde{x}_n . Specifically, the per-waveguide average SNR contribution is given by

$$\bar{\Gamma}_n(x, y; \tilde{x}_n) \triangleq \rho \frac{\eta \exp(-\beta r_n^2(x, y; \tilde{x}_n)) + \mu_n^2}{r_n^2(x, y; \tilde{x}_n)}. \quad (27)$$

Next, substituting the Gaussian-mixture traffic model (9) into (26) yields the hotspot decomposition

$$\begin{aligned} \tilde{f}_n(\tilde{x}_n) &= \iint_{\mathcal{D}} \bar{\Gamma}_n(x, y; \tilde{x}_n) \sum_{\ell=1}^L \alpha_{\ell} \mathcal{N}([x, y]^T; \boldsymbol{\mu}_{\ell}, \boldsymbol{\Sigma}_{\ell}) dx dy \\ &= \sum_{\ell=1}^L \alpha_{\ell} F_{n,\ell}(\tilde{x}_n), \end{aligned} \quad (28)$$

where

$$F_{n,\ell}(\tilde{x}_n) \triangleq \iint_{\mathcal{D}} \bar{\Gamma}_n(x, y; \tilde{x}_n) \mathcal{N}([x, y]^T; \boldsymbol{\mu}_{\ell}, \boldsymbol{\Sigma}_{\ell}) dx dy. \quad (29)$$

Here, $F_{n,\ell}(\tilde{x}_n)$ represents the contribution of hotspot ℓ to the per-waveguide objective along waveguide n , and (28) shows that $\tilde{f}_n(\cdot)$ is a traffic-weighted superposition of hotspot-induced component functions. This representation will serve as the starting point for the subsequent two-hotspot structural analysis.

1) *Shape of Each Hotspot-Induced Component $F_{n,\ell}(\tilde{x}_n)$:* We now study the structural properties of each hotspot-induced component $F_{n,\ell}(\tilde{x}_n)$ defined in (29). Throughout this subsubsection, we fix a waveguide index n and a hotspot index ℓ , and view $F_{n,\ell}(\cdot)$ as a scalar function of the pinching-antenna coordinate $\tilde{x}_n \in [0, D_x]$. For ease of analysis, we make the following assumption.

Assumption 1 *The hotspot centers $\{\mu_\ell\}_{\ell=1}^L$ lie well inside the service region $\mathcal{D} = [0, D_x] \times [-D_y/2, D_y/2]$, and the traffic density outside \mathcal{D} is negligible.*

Under Assumption 1, the key structural properties of each hotspot-induced component $F_{n,\ell}(\tilde{x}_n)$ are summarized in the following lemma.

Lemma 3 *Suppose that Assumption 1 holds. Then, for any waveguide n and hotspot ℓ , the function $F_{n,\ell}(\tilde{x}_n)$ defined in (29) is smooth and unimodal in \tilde{x}_n over $[0, D_x]$, and it attains its maximum at the hotspot horizontal center $\tilde{x}_n^* = \mu_{\ell,x}$.*

Proof: See Appendix B. ■

2) *Two-Hotspot Case: Merge–Split Behavior:* We now specialize to the two-hotspot case ($L = 2$) and study when the per-waveguide objective

$$\tilde{f}_n(x) = \alpha_1 F_{n,1}(x) + \alpha_2 F_{n,2}(x) \quad (30)$$

exhibits a *single* dominant peak (“merged” regime) or *two* distinct peaks (“split” regime). This characterization is useful because it explains why multimodality may arise even though each hotspot-induced component $F_{n,\ell}(x)$ is unimodal (Lemma 3), and it enables candidate-set construction that searches only a small number of informative points.

Since $f_n(x)$ is differentiable, any interior maximizer $x^* \in (0, D_x)$ must satisfy the first-order condition

$$\tilde{f}'_n(x^*) = \alpha_1 F'_{n,1}(x^*) + \alpha_2 F'_{n,2}(x^*) = 0. \quad (31)$$

Intuitively, (31) states that at an interior stationary point the (traffic-weighted) pull from hotspot 1 (through $F'_{n,1}$) is balanced by that from hotspot 2 (through $F'_{n,2}$).

Under Assumption 1 and Lemma 3, each component $F_{n,\ell}(x)$ is smooth and unimodal over $[0, D_x]$ with a unique maximizer at $x = \mu_{\ell,x}$. Hence, $F'_{n,\ell}(x) > 0$ for $x < \mu_{\ell,x}$ and $F'_{n,\ell}(x) < 0$ for $x > \mu_{\ell,x}$. Without loss of generality, assume $\mu_{1,x} < \mu_{2,x}$. Then, we have

$$\tilde{f}'_n(\mu_{1,x}) = \alpha_1 F'_{n,1}(\mu_{1,x}) + \alpha_2 F'_{n,2}(\mu_{1,x}) = \alpha_2 F'_{n,2}(\mu_{1,x}) > 0, \quad (32)$$

$$\tilde{f}'_n(\mu_{2,x}) = \alpha_1 F'_{n,1}(\mu_{2,x}) + \alpha_2 F'_{n,2}(\mu_{2,x}) = \alpha_1 F'_{n,1}(\mu_{2,x}) < 0. \quad (33)$$

By continuity of $f'_n(x)$ and the intermediate value theorem [32], there exists $x_b \in (\mu_{1,x}, \mu_{2,x})$ such that $f'_n(x_b) = 0$.

Although each $F_{n,\ell}$ is unimodal, the superposition f_n may be unimodal (merged regime) or bimodal (split regime). These behaviors are summarized in the following proposition.

Proposition 1 *Assume that Assumption 1 holds and $\mu_{1,x} < \mu_{2,x}$. Then, $\tilde{f}_n(x)$ has at least one stationary point in $(\mu_{1,x}, \mu_{2,x})$, i.e., there exists $x_b \in (\mu_{1,x}, \mu_{2,x})$ such that*

$\tilde{f}'_n(x_b) = 0$. Moreover, depending on the number of stationary points in $(\mu_{1,x}, \mu_{2,x})$, $\tilde{f}_n(x)$ exhibits the following regimes:

- 1) *(Merged regime)* If \tilde{f}_n has exactly one stationary point, denoted x_b , and $\tilde{f}''_n(x_b) < 0$, then \tilde{f}_n has a single dominant peak between the two hotspots; i.e., the maximizer of \tilde{f}_n over $[\mu_{1,x}, \mu_{2,x}]$ is unique and occurs at x_b .
- 2) *(Split regime)* If \tilde{f}_n has three stationary points in $(\mu_{1,x}, \mu_{2,x})$, denoted $x_L < x_M < x_R$, such that

$$\tilde{f}''_n(x_L) < 0, \quad \tilde{f}''_n(x_M) > 0, \quad \tilde{f}''_n(x_R) < 0, \quad (34)$$

then \tilde{f}_n has two distinct local maximizers x_L and x_R separated by a local minimizer x_M .

Proof: See Appendix C. ■

Proposition 1 suggests that, in the two-hotspot case, it suffices to compare $f_n(x)$ over a small candidate set formed by interior stationary points in $(\mu_{1,x}, \mu_{2,x})$ and (when relevant) the endpoints. A practical way to locate interior stationary points is to apply a *bracketing–bisection* procedure to the continuous derivative $h(x) \triangleq \tilde{f}'_n(x)$.

Step 1 (Bracket sign changes). Since h is continuous and satisfies $h(\mu_{1,x}) > 0$ and $h(\mu_{2,x}) < 0$, there exists at least one root in $(\mu_{1,x}, \mu_{2,x})$. To find *all* roots, discretize the interval into J subintervals:

$$x^{(0)} = \mu_{1,x} < x^{(1)} < \dots < x^{(J)} = \mu_{2,x}.$$

Evaluate $h(x^{(j)})$ for $j = 0, \dots, J$. For each adjacent pair $[x^{(j)}, x^{(j+1)}]$, if

$$h(x^{(j)}) h(x^{(j+1)}) < 0,$$

then by the intermediate value theorem there exists at least one root in $(x^{(j)}, x^{(j+1)})$; this interval is a *bracket* for a stationary point of f_n .

Step 2 (Bisection within each bracket). For each bracket $[a, b]$ with $h(a)h(b) < 0$, perform bisection: set $c = (a + b)/2$; if $h(a)h(c) \leq 0$ replace $b \leftarrow c$, else replace $a \leftarrow c$. Repeat until $|b - a| \leq \varepsilon$, and output $x^* \approx (a + b)/2$ as a stationary point.

Step 3 (Classify and build candidates). Compute $\tilde{f}''_n(x^*)$ (or use the sign change of h around x^*) to classify the stationary point as a local maximizer/minimizer, and add the maximizer-type points to the candidate set (merged: one point; split: two points).

Remark 1 *Note that the above algorithm development is based on the continuous model, which can still be computationally expensive, since evaluating $F_{n,\ell}(x)$ (and hence $f_n(x)$) requires computing a two-dimensional integral over \mathcal{D} (and doing so repeatedly for many trial points x during root-finding). This motivates the grid-based approximation adopted in (24), which replaces the continuous integral by a finite sum on Ω and yields a low-complexity surrogate that can be evaluated efficiently. Specifically, with the grid-based approximation, the stationary-point search in $(\mu_{1,x}, \mu_{2,x})$ can be implemented in a simple and robust coarse-to-fine manner like that in the above continuous model. The only difference is to replace $\tilde{f}_n(x)$ using its grid-based approximation $f_n(x)$*

defined in (24). Overall, this procedure avoids dense exhaustive search over $[0, D_x]$ while also eliminating repeated two-dimensional integrations, thereby enabling computationally efficient maximization in practice.

3) *Extension to the Multi-Hotspot Case:* For $L > 2$, the per-waveguide objective remains

$$f_n(x) = \sum_{\ell=1}^L \alpha_\ell F_{n,\ell}(x), \quad (35)$$

and any interior maximizer $x^* \in (0, D_x)$ must satisfy the equation

$$f'_n(x^*) = \sum_{\ell=1}^L \alpha_\ell F'_{n,\ell}(x^*) = 0. \quad (36)$$

Under Assumption 1 and Lemma 3, each $F_{n,\ell}(x)$ is smooth and unimodal with a unique maximizer at $x = \mu_{\ell,x}$, so $\tilde{f}_n(x)$ may admit multiple stationary points and, consequently, multi-peak profiles.

This observation motivates a scalable candidate-set construction: sort the hotspot centers $\mu_{(1),x} \leq \dots \leq \mu_{(L),x}$ and search for stationary points of f_n within each adjacent interval $(\mu_{(k),x}, \mu_{(k+1),x})$, $k = 1, \dots, L-1$, via coarse bracketing of sign changes in $\tilde{f}'_n(x)$ followed by bisection refinement. Collect the resulting stationary candidates and compare $\tilde{f}_n(x)$ only on this small set, instead of performing dense exhaustive search. In the grid-based model, the same procedure is applied to the discrete surrogate f_n and its analytical derivative f'_n , so that bracketing and candidate comparison can be carried out directly on the grid with low complexity.

IV. TRAFFIC-RESTRICTED MAX-MIN AVERAGE-SNR OPTIMIZATION

In this section, we consider a fairness-oriented design criterion that aims to enhance the worst covered part of the network, while explicitly taking into account the user traffic distribution. Instead of enforcing coverage uniformly over the entire communication area, including regions where users almost never appear, we restrict our attention to a set of active grids with sufficiently large traffic weights, and maximize the minimum local average SNR over this set by optimizing the pinching-antenna positions.

A. Active Grid Set and Problem Formulation

Recall from Section II-E that the communication region is discretized into grids indexed by

$$\Omega \triangleq \{1, \dots, N_h\} \times \{1, \dots, N_v\},$$

with grid centers $\psi_{u,v}$ and traffic weights $\{p_{u,v}\}_{(u,v) \in \Omega}$ obtained from the Gaussian hotspot model. Given a traffic threshold $p_{\text{th}} \in (0, 1)$, we define the active grid set as

$$\Omega_{\text{act}} \triangleq \{(u, v) \in \Omega : p_{u,v} \geq p_{\text{th}}\}, \quad (37)$$

which contains the grids where users appear with non-negligible probability. Grids with $p_{u,v} < p_{\text{th}}$ are excluded from the fairness criterion, so that the design is not dominated by extremely low-traffic regions.

The traffic-restricted worst-case average SNR is defined as

$$\Gamma_{\min}^{(\text{tr})}(\tilde{\mathbf{x}}) \triangleq \min_{(u,v) \in \Omega_{\text{act}}} \rho \sum_{n=1}^N \frac{\eta \exp(-\beta r_{n,u,v}^2(\tilde{x}_n)) + \mu_n^2}{r_{n,u,v}^2(\tilde{x}_n)}, \quad (38)$$

where $\bar{\Gamma}_{u,v}(\tilde{x})$, given in (19), is the local average SNR in grid (u, v) under deployment $\tilde{\mathbf{x}} = [\tilde{x}_1, \dots, \tilde{x}_N]^T$. $\Gamma_{\min}^{(\text{tr})}(\tilde{\mathbf{x}})$ measures the coverage quality of the most disadvantaged active grid.

Based on the above mode, the traffic-restricted max-min average SNR optimization problem is formulated as

$$\max_{\tilde{\mathbf{x}}} \Gamma_{\min}^{(\text{tr})}(\tilde{\mathbf{x}}) \quad (39a)$$

$$\text{s.t. } 0 \leq \tilde{x}_n \leq D_x, \quad \forall n \in \mathcal{N}. \quad (39b)$$

Problem (39) is, however, challenging to solve directly. First, the objective is a max-min of highly nonlinear functions of $\tilde{\mathbf{x}}$, since each $\bar{\Gamma}_{u,v}(\tilde{x})$ in (38) depends on the pinching-antenna positions through the distances $r_{n,u,v}(\tilde{x}_n)$ and the LoS probabilities $\exp(-\beta r_{n,u,v}^2(\tilde{x}_n))$, leading to a highly nonconvex landscape with potentially many local optima. Second, the outer minimum over $(u, v) \in \Omega_{\text{act}}$ introduces additional nonsmoothness, so that improving the average SNR of some grids may not immediately increase the worst-case value. Although global exhaustive or grid-search-based methods are still possible in principle, its computational complexity grows explosively with N_h , N_v , and N and quickly becomes prohibitive.

On the other hand, in the original formulation (39) the pinching-antenna positions are separable both in the average-SNR expressions and in the constraints. This structure naturally motivates a BCD approach. By updating one pinching-antenna position at a time and fixing the others, the multi-dimensional max-min problem is reduced to a sequence of one-dimensional subproblems, each with a simplified objective that can be handled much more efficiently.

B. BCD Method for the Original Max-Min Problem (39)

To handle the nonconvex, high-dimensional problem (39), we adopt a BCD strategy. At each iteration, we select one pinching antenna and adjust its position along the waveguide while keeping all other antennas fixed.

Let $\tilde{\mathbf{x}}^{(k)}$ denote the deployment at iteration k . From (38), the local average SNR in grid (u, v) can be decomposed as

$$\begin{aligned} \bar{\Gamma}_{u,v}(\tilde{\mathbf{x}}) &= \rho \sum_{m=1}^N \frac{\eta \exp(-\beta r_{m,u,v}^2(\tilde{x}_m)) + \mu_m^2}{r_{m,u,v}^2(\tilde{x}_m)} \\ &= A_{u,v}^{(-n)} + g_{n,u,v}(\tilde{x}_n), \quad (u, v) \in \Omega, \end{aligned} \quad (40)$$

where

$$A_{u,v}^{(-n)} \triangleq \rho \sum_{\substack{m=1 \\ m \neq n}}^N \frac{\eta \exp(-\beta r_{m,u,v}^2(\tilde{x}_m^{(k)})) + \mu_m^2}{r_{m,u,v}^2(\tilde{x}_m^{(k)})}, \quad (41)$$

$$g_{n,u,v}(x) \triangleq \rho \frac{\eta \exp(-\beta r_{n,u,v}^2(\tilde{x}_n)) + \mu_n^2}{r_{n,u,v}^2(\tilde{x}_n)}. \quad (42)$$

Here, $A_{u,v}^{(-n)}$ collects the contribution of all antennas except n and is fixed during the update of \tilde{x}_n , while $g_{n,u,v}(\tilde{x}_n)$ captures the contribution of antenna n as a function of its position \tilde{x}_n .

Substituting (40) into (38), and fixing $\{\tilde{x}_m^{(k)}\}_{m \neq n}$, the original traffic-restricted max-min objective becomes a one-dimensional function of \tilde{x}_n , which is given by

$$\Gamma_{\min}^{(\text{tr})}(\tilde{x}_n) = \min_{(u,v) \in \Omega_{\text{act}}} (A_{u,v}^{(-n)} + g_{n,u,v}(\tilde{x}_n)). \quad (43)$$

Therefore, the BCD update for antenna n at iteration k is given by the one-dimensional max-min subproblem

$$\max_{0 \leq \tilde{x}_n \leq D_x} F_n^{(\text{tr})}(\tilde{x}_n) \triangleq \min_{(u,v) \in \Omega_{\text{act}}} (A_{u,v}^{(-n)} + g_{n,u,v}(\tilde{x}_n)). \quad (44)$$

As seen, starting directly from the original max-min formulation (39), the BCD scheme is naturally motivated. For each antenna, we move its pinching position along the waveguide to improve the worst local average SNR over all active grids, while the contributions of the other antennas remain fixed in $A_{u,v}^{(-n)}$. In what follows, we show that each one-dimensional subproblem can be globally solved using a low-complexity bisection-based algorithm.

C. Epigraph Reformulation and Bisection-Based Method for the One-Dimensional Subproblem (44)

Although the coordinate subproblem (44) is one-dimensional, it remains nonconvex due to the max-min structure. Our key observation is that, under the smooth average-SNR model (40)–(42), the feasibility set induced by each grid constraint has an interval structure, and the overall feasibility reduces to an interval intersection test. This converts the global solution of the nonconvex one-dimensional max-min problem into a low-complexity nested bisection routine.

For a fixed antenna n and given $\{A_{u,v}^{(-n)}\}$, the one-dimensional subproblem (44) admits the following epigraph reformulation:

$$\max_{0 \leq \tilde{x}_n \leq D_x, t} t \quad (45a)$$

$$\text{s.t. } A_{u,v}^{(-n)} + g_{n,u,v}(\tilde{x}_n) \geq t, \forall (u,v) \in \Omega_{\text{act}}, \quad (45b)$$

where t represents the worst local average SNR over the active grids under the current update of antenna n . While (45) is still nonconvex, its *global* optimum can be obtained efficiently by exploiting the monotone feasibility structure in t , as summarized below.

Proposition 2 Fix antenna n and $\{A_{u,v}^{(-n)}\}$. For each $(u,v) \in \Omega_{\text{act}}$, define the per-grid feasibility set

$$\mathcal{X}_{u,v}(t) \triangleq \left\{ \tilde{x}_n \in [0, D_x] \mid A_{u,v}^{(-n)} + g_{n,u,v}(\tilde{x}_n) \geq t \right\}, \quad (46)$$

and the overall feasibility set

$$\mathcal{X}_n^{(\text{tr})}(t) \triangleq \bigcap_{(u,v) \in \Omega_{\text{act}}} \mathcal{X}_{u,v}(t). \quad (47)$$

Then, the following properties hold

TABLE I: Default simulation parameters.

Parameter	Value
Carrier frequency (f_c)	28 GHz
Communication-region size ($D_x \times D_y$)	60×200 m 2
Waveguide height (d_v)	10 m
Transmit power (P)	40 dBm
Noise power (σ^2)	-70 dBm
NLoS power (μ^2)	-60 dBm
Number of PAs / waveguides (N)	6
Number of grids ($N_h \times N_v$)	400×120
LoS blockage parameter (β)	0.01
Algorithm tolerance (ϵ_t, ϵ_d)	10^{-3}
Number of hotspots (L)	3
Active-set threshold (p_{th})	$0.02 \times \max_{u,v} \{p_{u,v}\}$

1) (Interval structure). For each $(u,v) \in \Omega_{\text{act}}$, $\mathcal{X}_{u,v}(t)$ is either empty or a (possibly clipped) interval in $[0, D_x]$ of the form $[x_u - d_{u,v}(t), x_u + d_{u,v}(t)] \cap [0, D_x]$, where $d_{u,v}(t) \geq 0$ is uniquely determined by

$$A_{u,v}^{(-n)} + g_{n,u,v}(x_u + d_{u,v}(t)) = t. \quad (48)$$

Consequently, $\mathcal{X}_n^{(\text{tr})}(t)$ is either empty or an interval in $[0, D_x]$.

2) (Nestedness). For any $t_1 \leq t_2$, we have $\mathcal{X}_{u,v}(t_2) \subseteq \mathcal{X}_{u,v}(t_1)$ for all $(u,v) \in \Omega_{\text{act}}$, and hence $\mathcal{X}_n^{(\text{tr})}(t_2) \subseteq \mathcal{X}_n^{(\text{tr})}(t_1)$.

3) (Threshold optimality). Define $t_n^* \triangleq \sup \{t \mid \mathcal{X}_n^{(\text{tr})}(t) \neq \emptyset\}$. Then, $\mathcal{X}_n^{(\text{tr})}(t) \neq \emptyset$ for all $t < t_n^*$ and $\mathcal{X}_n^{(\text{tr})}(t) = \emptyset$ for all $t > t_n^*$. Moreover, t_n^* equals the optimal objective value of (45), and any $\tilde{x}_n^* \in \mathcal{X}_n^{(\text{tr})}(t_n^*)$ is an optimal solution.

The proof of proposition 2 follows similar idea of the proof for [26, Propistion 1], thus we omit it here due to the space limitation. The properties established in Proposition 2 enable an efficient global solution method for (45). In particular, the monotone nesting of $\mathcal{X}_n^{(\text{tr})}(t)$ allows t_n^* to be computed via a scalar bisection search over t . At each bisection iteration, we fix a candidate t , construct the per-grid feasible intervals $\{\mathcal{X}_{u,v}(t)\}$ by solving the defining scalar equation for $d_{u,v}(t)$, form their intersection $\mathcal{X}_n^{(\text{tr})}(t)$ according to (47), and declare t feasible if $\mathcal{X}_n^{(\text{tr})}(t) \neq \emptyset$. By iteratively shrinking the search range based on this feasibility test, we obtain t_n^* and a corresponding optimal \tilde{x}_n^* with low complexity. This bisection-based solver is then used as the inner routine for each coordinate update in the overall BCD algorithm.

V. SIMULATION RESULTS

In this section, numerical simulations are presented to validate the performance of proposed algorithms for the traffic-aware pinching-antenna system designs. The main simulation parameters are listed in Table I. Unless otherwise stated, the default values in Table I are adopted. All curves are obtained by averaging over 100 independent traffic realizations, each consisting of three randomly placed hotspots. The spatial traffic distribution is modeled as a three-component Gaussian mixture: for each realization, the hotspot centers are drawn

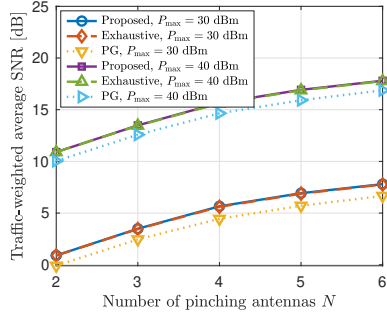


Fig. 2: Traffic-weighted network average-SNR performance comparison among the proposed algorithm with two baselines.

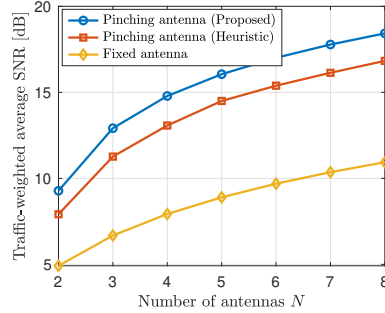


Fig. 3: Traffic-aware network average SNR comparisons between different schemes versus the number of antennas N .

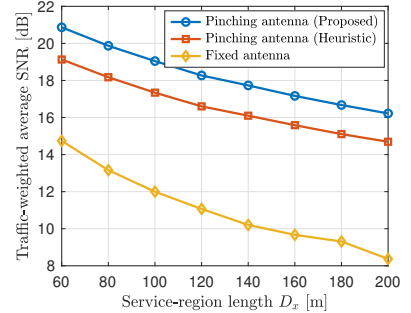


Fig. 4: Traffic-aware network average-SNR comparisons between different schemes versus the communication-region length D_x .

TABLE II: Execution time (in seconds) of the considered algorithms.

		$\Delta x = \lambda/5, J = 10, K_{\max} = 30$				
		$N = 2$	$N = 3$	$N = 4$	$N = 5$	$N = 6$
Exhaustive	7.83	11.71	15.6	19.56	23.43	
	0.034	0.048	0.059	0.073	0.089	
	0.030	0.044	0.060	0.070	0.085	
		$\Delta x = \lambda/10, J = 20, K_{\max} = 50$				
		$N = 2$	$N = 3$	$N = 4$	$N = 5$	$N = 6$
Exhaustive	15.61	23.35	30.88	38.66	46.61	
	0.033	0.049	0.064	0.077	0.098	
	0.044	0.072	0.096	0.130	0.159	

uniformly from $[0, D_x] \times [-D_y/2, D_y/2]$, the mixture weights are independently generated and then normalized to sum to one, and all components share the same covariance matrix $\Sigma = \text{diag}((0.15D_x)^2, (0.2D_y)^2)$.

A. Performance of the Traffic-Aware Network Average SNR Optimization

We first assess the global optimality of the proposed method by benchmarking it against the exhaustive search baseline in Fig. 2, and also include a projected gradient (PG) method as a representative local-optimization approach. Exploiting the separable structure $\bar{\Gamma}_{\text{net}} = \sum_{n=1}^N f_n(\tilde{x}_n)$, all three schemes reduce the design to N independent one-dimensional maximization problems. For the exhaustive baseline, we conduct a dense linear search over $[0, D_x]$ with a uniform step size $\Delta_x = \lambda/5$ and choose the best grid point. For the proposed method, we partition $[0, D_x]$ into $J = 10$ coarse subintervals to detect sign changes of $f'_n(x)$, refine each bracketed root via bisection, and then evaluate $f_n(x)$ only at the resulting stationary-point candidates (and endpoints when relevant). For PG, we iteratively update \tilde{x}_n along the gradient direction with step-size control and projection onto $[0, D_x]$ with maximum iterations of $K_{\max} = 30$. As seen in Fig. 2, the proposed method overlaps with the exhaustive search for both $P_{\max} = 30$ dBm and 40 dBm across all N , confirming that the candidate-based search achieves the same objective value as exhaustive linear search in this experiment while avoiding dense scanning. In contrast, PG yields consistently lower values, since it is sensitive to initialization and may converge to suboptimal

stationary points in this nonconvex setting. Moreover, the traffic-weighted average SNR increases with N but exhibits diminishing returns, and a larger P_{\max} consistently shifts the curves upward.

Table II further reports the average execution time of the three methods under two parameter settings: $\Delta x = \lambda/5, J = 10, K_{\max} = 30$ and $\Delta x = \lambda/10, J = 20, K_{\max} = 50$. In both settings, all methods exhibit an approximately increasing runtime with N , since they solve N decoupled one-dimensional subproblems. Several clear trends can be observed. First, the exhaustive linear search is the most time-consuming, because it must evaluate $f_n(x)$ over a dense grid on $[0, D_x]$ and the number of grid points scales inversely with Δx . Second, the proposed candidate-based method is consistently orders of magnitude faster than exhaustive search, since it avoids dense scanning and instead relies on coarse sign-change bracketing followed by only a small number of bisection refinements. Third, the PG method has comparable runtime to the proposed method in the first setting, but becomes noticeably slower in the second setting due to the larger iteration budget ($K_{\max} = 50$). Overall, Table II confirms that the proposed approach offers a substantial computational advantage over exhaustive search, while remaining competitive with PG and additionally providing candidate-based global maximization for each one-dimensional subproblem.

To quantify both the benefit of adopting pinching antennas and the extra gain from traffic-aware position optimization, Fig. 3 compares the proposed design with two baselines. The first is a simple hotspot-center heuristic that places each pinching antenna at a hotspot's geometric center, representing coarse traffic-informed deployment. The second is a fixed-antenna benchmark that uses an N -element half-wavelength-spaced array centered at $x = D_x/2$ (with $\lambda/2$ spacing along y), representing a traffic-agnostic, non-reconfigurable design. As shown in Fig. 3, the proposed method achieves the highest network average SNR for all N , verifying the value of directly optimizing antenna locations under the traffic-weighted objective. The heuristic notably outperforms the fixed benchmark, but remains below PG since it does not optimize the global metric, while the fixed benchmark performs the worst due to its lack of adaptability to hotspot locations.

To study how the gain of pinching antennas and the extra gain from traffic-aware position optimization scales with the

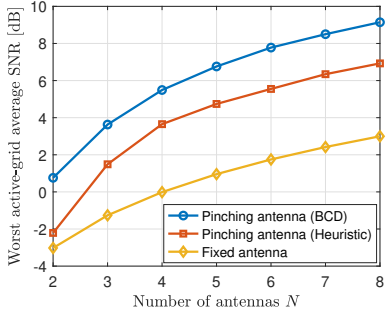


Fig. 5: Worst active-grid average SNR comparisons with baselines versus the number of antennas N for the traffic-restricted max-min design.

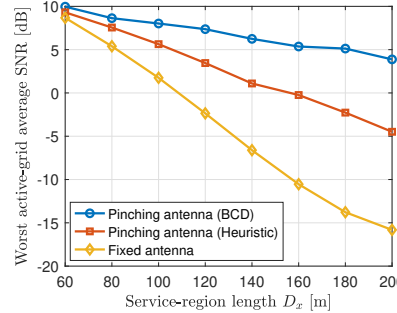


Fig. 6: Worst active-grid average SNR comparisons with baselines versus the communication-region length D_x for the traffic-restricted max-min design.

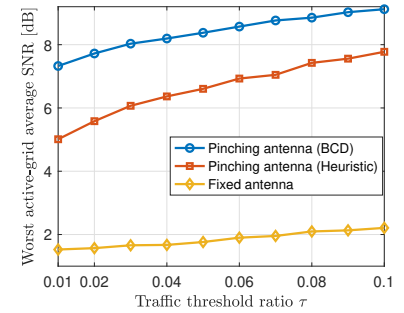


Fig. 7: Worst active-grid average SNR comparisons with baselines versus the traffic threshold ratio τ for the traffic-restricted max-min design.

service-region length, Fig. 4 compares the proposed design with the two baselines as D_x varies. As D_x increases, the network average SNR decreases for all schemes because the typical propagation distance grows, degrading link quality over the traffic field. Nevertheless, the proposed design consistently performs best across the entire D_x range, demonstrating the robustness of traffic-aware optimization as the coverage area expands. The heuristic hotspot-center deployment remains competitive and clearly outperforms the fixed benchmark, confirming that even simple traffic-informed placement is beneficial, but it is still inferior to the proposed method since it does not optimize the global traffic-weighted objective. Moreover, the gap between the pinching-antenna designs and the fixed benchmark widens with D_x , indicating that placement adaptability becomes increasingly valuable in larger service regions.

B. Performance of the Traffic-Restricted Max-Min Average SNR Optimization

To illustrate the gain from pinching antennas and traffic-aware positioning, Fig. 5 compares the proposed BCD-based design with two baselines (set following Fig. 3). The BCD solution consistently achieves the highest worst active-grid average SNR for all N , validating explicit optimization under the traffic-restricted max-min objective. The hotspot-center heuristic improves upon the fixed benchmark but remains inferior because it does not balance SNR across active grids. The fixed benchmark performs worst due to its traffic-agnostic, non-adaptive placement, which leaves a more severe bottleneck grid. Fig. 6 studies how the pinching-antenna gain (and the extra gain from position optimization) changes with the service-region length D_x . The worst active-grid average SNR decreases with D_x for all schemes due to larger typical propagation distances and a more challenging bottleneck in the active set. Still, the proposed BCD-based design consistently performs best over the entire D_x range, showing its effectiveness in sustaining the worst-grid SNR as coverage expands. The hotspot-center heuristic degrades faster since it does not directly optimize the bottleneck, while the fixed benchmark suffers the largest loss, underscoring the poor robustness of traffic-agnostic, geometry-constrained deployments in large regions.

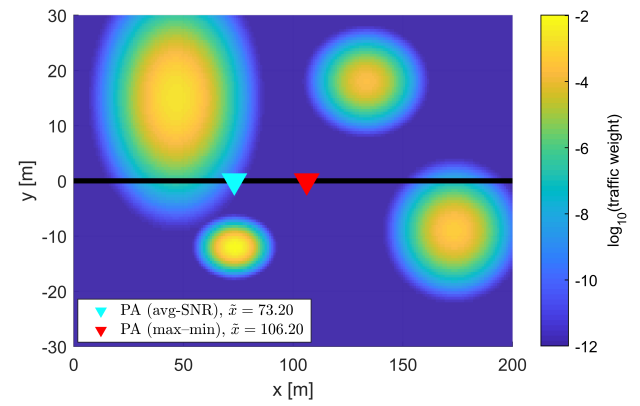


Fig. 8: Top-view illustration of the optimized pinching-antenna position under the network average-SNR maximization and the traffic-restricted max-min average-SNR maximization objectives for a fixed four-hotspot traffic field with a single waveguide at $\tilde{y} = 0$.

Fig. 7 evaluates how the traffic-restricted max-min design varies with the active-set threshold $p_{\text{th}} = \tau \max_{u,v} p_{u,v}$, where τ controls how selectively traffic-dominant grids are included. As τ increases, the worst active-grid average SNR generally improves for all schemes because the active set becomes smaller and more concentrated on heavily loaded locations, easing the bottleneck. Throughout the entire τ range, the proposed BCD-based pinching-antenna design consistently achieves the highest worst active-grid SNR, showing that traffic-aware position optimization remains effective under different active-set definitions. The hotspot-center heuristic follows the same trend but stays noticeably below BCD since it does not explicitly balance the SNR across the active grids, while the fixed benchmark performs worst and is least robust to traffic-dependent selection.

Fig. 8 illustrates how different traffic-aware objectives can yield different pinching-antenna placements under the same setting. We consider a single-waveguide scenario with $\tilde{y} = 0$ and one pinching antenna whose location $\tilde{x} \in [0, D_x]$ is optimized. The background heatmap shows the normalized traffic weights $p_{u,v}$ from a four-hotspot Gaussian-mixture field. For this fixed traffic map, we compute (i) the network average-SNR maximization solution (via the projected-gradient method) and (ii) the traffic-restricted max-min average-SNR solution (over the active set Ω_{act} defined

by the traffic threshold), and mark both locations on the waveguide. As seen in Fig. 8, the average-SNR design moves the antenna closer to the highest-traffic region to boost traffic-weighted efficiency, whereas the traffic-restricted max-min design shifts toward a more “balancing” position to improve the worst SNR within Ω_{act} . This contrast reflects the underlying philosophies: traffic-proportional averaging versus bottleneck-aware robustness within the active region.

VI. CONCLUSION

In this paper (Part I), we investigated traffic-aware network-level design for generalized pinching-antenna systems. To move beyond link-level optimization tied to instantaneous user geometry, we introduced a tractable spatial-traffic modeling framework and defined traffic-aware performance metrics based on traffic-weighted spatial aggregation of the local average SNR. A grid-based discretization was further developed to obtain numerically efficient discrete counterparts of the continuous-domain metrics. Building on these models, we formulated two traffic-aware deployment problems: maximizing the traffic-weighted network average SNR and a fairness-oriented traffic-restricted max-min average-SNR design over traffic-dominant grids. Efficient low-complexity algorithms were proposed, including a candidate-based global optimization algorithm for the traffic-weighted objective and a BCD method with bisection-based coordinate updates for the max-min objective. Numerical results demonstrated fast convergence and showed that the proposed traffic-aware designs can outperform representative fixed and heuristic baselines under the considered scenarios, while also revealing how the achievable gains and robustness-efficiency tradeoffs depend on the traffic heterogeneity and system parameters.

APPENDIX A PROOF OF LEMMA 1

According to the random LoS/NLoS channel model, the channel coefficient of n -th pinching antenna is given by

$$h_n(\psi_{u,v}, \tilde{\mathbf{x}}) = \gamma_n h_n^{\text{LoS}}(\psi_{u,v}, \tilde{\mathbf{x}}) + h_n^{\text{NLoS}}(\psi_{u,v}, \tilde{\mathbf{x}}), \quad (49)$$

where $\gamma_n \in \{0, 1\}$ is the LoS indicator, and the LoS probability is given by

$$\Pr[\gamma_n = 1] = \exp(-\beta r_{n,u,v}^2(\tilde{\mathbf{x}})). \quad (50)$$

From the LoS expression in Section II-B, we have

$$|h_n^{\text{LoS}}(\psi_{u,v}, \tilde{\mathbf{x}})|^2 = \frac{\eta}{r_{n,u,v}^2(\tilde{\mathbf{x}})}. \quad (51)$$

For the NLoS component, we have

$$\mathbb{E}[|h_n^{\text{NLoS}}(\psi_{u,v}, \tilde{\mathbf{x}})|^2] = \frac{\mu_n^2}{r_{n,u,v}^2(\tilde{\mathbf{x}})}. \quad (52)$$

Using the independence between γ_n and h_n^{NLoS} , and the zero mean of the NLoS term, the average channel power contributed by the n -th pinching antenna to grid (u, v) gives

$$\begin{aligned} \bar{G}_{n,u,v}(\tilde{\mathbf{x}}) &\triangleq \mathbb{E}[|h_n(\psi_{u,v}, \tilde{\mathbf{x}})|^2] \\ &= \mathbb{E}[\gamma_n] |h_n^{\text{LoS}}(\psi_{u,v}, \tilde{\mathbf{x}})|^2 + \mathbb{E}[|h_n^{\text{NLoS}}(\psi_{u,v}, \tilde{\mathbf{x}})|^2] \end{aligned}$$

$$= \frac{\eta \exp(-\beta r_{n,u,v}^2(\tilde{\mathbf{x}})) + \mu_n^2}{r_{n,u,v}^2(\tilde{\mathbf{x}})}. \quad (53)$$

Therefore, the local average SNR in grid (u, v) is

$$\begin{aligned} \bar{\Gamma}_{u,v}(\tilde{\mathbf{x}}) &\triangleq \mathbb{E}[\Gamma_{u,v}(\tilde{\mathbf{x}})] \\ &= \rho \sum_{n=1}^N \bar{G}_{n,u,v}(\tilde{\mathbf{x}}) \\ &= \rho \sum_{n=1}^N \frac{\eta \exp(-\beta r_{n,u,v}^2(\tilde{\mathbf{x}})) + \mu_n^2}{r_{n,u,v}^2(\tilde{\mathbf{x}})}. \end{aligned} \quad (54)$$

Using (17), the traffic-aware network average SNR can now be written as (20). The proof is The proof is complete.. ■

APPENDIX B PROOF OF LEMMA 3

First, let $(X_\ell, Y_\ell) \sim \mathcal{N}(\mu_\ell, \Sigma_\ell)$. Under Assumption 1 and by the definition of expectation under a PDF, (29) can be written as

$$F_{n,\ell}(\tilde{x}_n) = \mathbb{E}_{X_\ell, Y_\ell} [\bar{\Gamma}_n(X_\ell, Y_\ell; \tilde{x}_n)]. \quad (55)$$

Then, by defining the scalar mapping $k_n(s) \triangleq \rho \frac{\eta e^{-\beta s} + \mu_n^2}{s}$, $s > 0$ and using (27), we can rewrite the per-waveguide average SNR as $\bar{\Gamma}_n(x, y; \tilde{x}_n) = k_n(r_n^2(x, y; \tilde{x}_n))$. Moreover, $k_n(s)$ is strictly decreasing on $s > 0$ because both $e^{-\beta s}/s$ and $1/s$ are strictly decreasing for $s > 0$. Since Σ_ℓ is diagonal, X_ℓ and Y_ℓ are independent. Fix $t \geq 0$ and define

$$\phi_{n,\ell}(t) \triangleq \mathbb{E}_{Y_\ell} [k_n(t + (\tilde{y}_n - Y_\ell)^2 + d_v^2)], \quad (56)$$

where the expectation is taken with respect to $Y_\ell \sim \mathcal{N}(\mu_{\ell,y}, \sigma_{\ell,y}^2)$. Since $k_n(\cdot)$ is strictly decreasing, $\phi_{n,\ell}(t)$ is also strictly decreasing on $t \geq 0$. Now, applying the law of iterated expectation to (55) gives

$$\begin{aligned} F_{n,\ell}(\tilde{x}_n) &= \mathbb{E}_{X_\ell} [\mathbb{E}_{Y_\ell} [k_n((\tilde{x}_n - X_\ell)^2 + (\tilde{y}_n - Y_\ell)^2 + d_v^2)]] \\ &= \mathbb{E}_{X_\ell} [\phi_{n,\ell}((\tilde{x}_n - X_\ell)^2)]. \end{aligned} \quad (57)$$

Define $g_{n,\ell}(u) \triangleq \phi_{n,\ell}(u^2)$, $u \in \mathbb{R}$. Then $g_{n,\ell}(u)$ is even (i.e., $g_{n,\ell}(u) = g_{n,\ell}(-u)$) and strictly decreasing in $|u|$ because $\phi_{n,\ell}(t)$ is strictly decreasing in t . Let f_{X_ℓ} denote the PDF of $X_\ell \sim \mathcal{N}(\mu_{\ell,x}, \sigma_{\ell,x}^2)$. Writing the expectation in (57) as an integral yields

$$\begin{aligned} F_{n,\ell}(\tilde{x}_n) &= \int_{-\infty}^{\infty} \phi_{n,\ell}((\tilde{x}_n - \xi)^2) f_{X_\ell}(\xi) d\xi \\ &= \int_{-\infty}^{\infty} g_{n,\ell}(\tilde{x}_n - \xi) f_{X_\ell}(\xi) d\xi \\ &= (g_{n,\ell} * f_{X_\ell})(\tilde{x}_n), \end{aligned} \quad (58)$$

where $(g * f)(x) \triangleq \int g(x - \xi) f(\xi) d\xi$ denotes convolution.

Since $g_{n,\ell}$ is symmetric unimodal and f_{X_ℓ} is Gaussian (thus symmetric unimodal), their convolution is unimodal (e.g., [33, Theorem 2.1]). We next show it is symmetric about $\mu_{\ell,x}$. Letting $\tilde{x}_n = \mu_{\ell,x} + z$ and changing variables $\xi = \mu_{\ell,x} + t$, we have

$$\begin{aligned} F_{n,\ell}(\mu_{\ell,x} + z) &= \int_{-\infty}^{\infty} g_{n,\ell}(z - t) f_0(t) dt \\ &\stackrel{(a)}{=} \int_{-\infty}^{\infty} g_{n,\ell}(-(z - t)) f_0(t) dt \end{aligned}$$

$$\begin{aligned}
& \stackrel{(b)}{=} \int_{-\infty}^{\infty} g_{n,\ell}(-z+t) f_0(t) dt \\
& \stackrel{(c)}{=} \int_{-\infty}^{\infty} g_{n,\ell}(-z-t) f_0(-t) dt \\
& \stackrel{(d)}{=} \int_{-\infty}^{\infty} g_{n,\ell}(-z-t) f_0(t) dt \\
& = F_{n,\ell}(\mu_{\ell,x} - z), \tag{59}
\end{aligned}$$

where where $f_0(t) \triangleq f_{X_\ell}(\mu_{\ell,x} + t)$ is even and $g_{n,\ell}$ is even, (a) uses the evenness of $g_{n,\ell}(\cdot)$, i.e., $g_{n,\ell}(u) = g_{n,\ell}(-u)$, (b) uses $-(z-t) = -z+t$, (c) applies the change of variable $t \mapsto -t$, and (d) uses the evenness of $f_0(\cdot)$, i.e., $f_0(t) = f_0(-t)$. Hence $F_{n,\ell}$ is symmetric about $\mu_{\ell,x}$ and, being unimodal, achieves its maximum at $\tilde{x}_n = \mu_{\ell,x}$. The proof is complete. ■

APPENDIX C PROOF OF PROPOSITION 1

The existence of the stationary point follows from (32)–(33) and the intermediate value theorem applied to the continuous function $\tilde{f}'_n(x)$ on $[\mu_{1,x}, \mu_{2,x}]$.

For merge regime, if x_b is the unique stationary point in $(\mu_{1,x}, \mu_{2,x})$ and satisfies $f_n''(x_b) < 0$, then x_b is a strict local maximizer. Moreover, since $\tilde{f}'_n(\mu_{1,x}) > 0$ and $\tilde{f}'_n(\mu_{2,x}) < 0$, the derivative must change sign from positive to negative across $(\mu_{1,x}, \mu_{2,x})$. Uniqueness of the stationary point forces this sign change to occur at x_b , implying that \tilde{f}_n is increasing on $[\mu_{1,x}, x_b]$ and decreasing on $[x_b, \mu_{2,x}]$. Hence, x_b is the unique maximizer of \tilde{f}_n over $[\mu_{1,x}, \mu_{2,x}]$.

For split regime, the second-order conditions imply that x_L and x_R are strict local maximizers while x_M is a strict local minimizer. Since $x_L < x_M < x_R$, the two maximizers are distinct and are separated by a valley at x_M , yielding a two-peak (split) structure on $(\mu_{1,x}, \mu_{2,x})$. ■

REFERENCES

- [1] Z. Niu, “TANGO: traffic-aware network planning and green operation,” *IEEE Wireless Commun.*, vol. 18, no. 5, pp. 25–29, Oct. 2011.
- [2] Y. Zeng and X. Xu, “Toward environment-aware 6G communications via channel knowledge map,” *IEEE Wireless Commun.*, vol. 28, no. 3, pp. 84–91, Jun. 2021.
- [3] S. Bi, J. Lyu, Z. Ding, and R. Zhang, “Engineering radio maps for wireless resource management,” *IEEE Wireless Commun.*, vol. 26, no. 2, pp. 133–141, Apr. 2019.
- [4] B. Partov, D. J. Leith, and R. Razavi, “Utility fair optimization of antenna tilt angles in LTE networks,” *IEEE/ACM Trans. Networking*, vol. 23, no. 1, pp. 175–185, Feb 2015.
- [5] V. Buenestado, M. Toril, S. Luna-Ramírez, J. M. Ruiz-Avilés, and A. Mendo, “Self-tuning of remote electrical tilts based on call traces for coverage and capacity optimization in lte,” *IEEE Trans. Veh. Technol.*, vol. 66, no. 5, pp. 4315–4326, May 2017.
- [6] Y. Zeng, J. Chen, J. Xu, D. Wu, X. Xu, S. Jin, X. Gao, D. Gesbert, S. Cui, and R. Zhang, “A tutorial on environment-aware communications via channel knowledge map for 6G,” *IEEE Commun. Surv. Tutorials*, vol. 26, no. 3, pp. 1478–1519, thirdquarter 2024.
- [7] L. Li, Y. Xu, Y. Xue, F. Yin, C. Shen, R. Zhang, and T.-H. Chang, “PEMNet: Towards autonomous and enhanced environment-aware mobile networks,” *IEEE Commun. Mag. (submitted)*, 2026, available online: arXiv:2601.11025.
- [8] Z.-Q. Luo, X. Zheng, D. López-Pérez, Q. Yan, X. Chen, N. Wang, Q. Shi, T.-H. Chang, and A. García-Rodríguez, “SRCON: A data-driven network performance simulator for real-world wireless networks,” *IEEE Commun. Mag.*, vol. 61, no. 6, pp. 96–102, Jun. 2023.
- [9] B. Peng, S. Zhang, X. Zheng, Y. Xue, X. Qin, and T.-H. Chang, “RF-LSCM: Pushing radiance fields to multi-domain localized statistical channel modeling for cellular network optimization,” 2025, arXiv preprint arXiv:2509.13686.
- [10] Y. Xu, J. Cui, Y. Zhu, Z. Ding, T.-H. Chang, R. Schober, V. W. Wong, O. A. Dobre, G. K. Karagiannidis, H. V. Poor, and X. You, “Generalized pinching-antenna systems: A tutorial on principles, design strategies, and future directions,” *IEEE Commun. Surv. Tutorials (submitted)*, 2025, Available online: arXiv:2510.14166.
- [11] A. Fukuda, H. Yamamoto, H. Okazaki, Y. Suzuki, and K. Kawai, “Pinching antenna: Using a dielectric waveguide as an antenna,” *NTT DOCOMO Technical J.*, Jan. 2022.
- [12] Z. Ding, R. Schober, and H. V. Poor, “Flexible-antenna systems: A pinching-antenna perspective,” *IEEE Trans. Commun.*, vol. 73, no. 10, pp. 9236–9253, 2025.
- [13] Y. Xu, Z. Ding, and G. K. Karagiannidis, “Rate maximization for downlink pinching-antenna systems,” *IEEE Wireless Commun. Lett.*, vol. 14, no. 5, pp. 1431–1435, May 2025.
- [14] A. Bereyhi, C. Ouyang, S. Asaad, Z. Ding, and H. V. Poor, “MIMO-PASS: Uplink and downlink transmission via MIMO pinching-antenna systems,” *arXiv preprint arXiv:2503.03117*, 2025.
- [15] L. Zhang, X. Mu, A. Liu, and Y. Liu, “Two-timescale joint transmit and pinching beamforming for pinching-antenna systems,” *IEEE Wireless Commun. Lett.*, pp. 1–1, 2025.
- [16] P. Papanikolaou, D. Bozanis, S. A. Tegos, P. D. Diamantoulakis, P. Sarigiannidis, and G. K. Karagiannidis, “Physical layer security with artificial noise in MIMO pinching-antenna systems,” 2025, available online: arXiv:2511.23079.
- [17] K. Zhou, W. Zhou, D. Cai, X. Lei, Y. Xu, Z. Ding, and P. Fan, “A gradient meta-learning joint optimization for beamforming and antenna position in pinching-antenna systems,” *IEEE Trans. Commun.*, vol. 74, pp. 1099–1112, 2026.
- [18] K. Wang, Z. Ding, and G. K. Karagiannidis, “Antenna activation and resource allocation in multi-waveguide pinching-antenna systems,” *IEEE Trans. Wireless Commun.*, vol. 25, pp. 4070–4082, 2026.
- [19] N. Vashakidze, C. Assi, M. Elhattab, A. Ghayeb, and M. J. Khabbaz, “Joint power allocation and radiation optimization in NOMA-assisted pinching antenna systems,” 2025, available online: arXiv:2511.04861.
- [20] S. Xue, J. Zhao, K. Cai, X. Mu, Z. Xiao, and Y. Liu, “Resource allocation for pinching-antenna systems (PASS)-enabled NOMA communications,” 2025, available online: arXiv:2512.03502.
- [21] Z. Ding, “Pinching-antenna assisted ISAC: A CRLB perspective,” 2025, arXiv preprint arXiv:2504.05792.
- [22] A. Khalili, B. Kaziu, V. K. Papanikolaou, and R. Schober, “Pinching antenna-enabled ISAC systems: Exploiting look-angle dependence of RCS for target diversity,” 2025, arXiv preprint arXiv:2505.01777.
- [23] W. Mao, Y. Lu, Y. Xu, B. Ai, O. A. Dobre, and D. Niyato, “Multi-waveguide pinching antennas for ISAC,” *IEEE Trans. Wireless Commun.*, vol. 25, pp. 5846–5858, 2026.
- [24] Z. Ding, R. Schober, and H. V. Poor, “Environment division multiple access (EDMA): A feasibility study via pinching antennas,” 2025, available online: arXiv:2511.03820.
- [25] K. Wang, Z. Ding, and L. Hanzo, “Generalized pinching-antenna systems: A leaky-coaxial-cable perspective,” 2025, Available online: arXiv:2510.14166.
- [26] Y. Xu, Y. Lu, Z. Ding, and T.-H. Chang, “Pinching-antenna system design under random LoS and NLoS channels,” *IEEE Trans. Wireless Commun. (submitted)*, 2025, available online: arXiv:2512.04719.
- [27] Y. Xu, Z. Ding, R. Schober, and T.-H. Chang, “Pinching-antenna systems with in-waveguide attenuation: Performance analysis and algorithm design,” *IEEE Trans. Wireless Commun. (submitted)*, 2025, available online: arXiv:2506.23966.
- [28] Y. Xu, Z. Ding, O. A. Dobre, and T.-H. Chang, “Pinching-antenna system design with LoS blockage: Does in-waveguide attenuation matter?” *IEEE Trans. Wireless Commun. (submitted)*, 2025, available online: arXiv:2508.07131.
- [29] 3GPP, “Study on channel model for frequencies from 0.5 to 100 GHz,” 3GPP TR 38.901 version 16.1.0 Release 16, Tech. Rep., 2020.
- [30] T. Bai, R. Vaze, and R. W. Heath, “Analysis of blockage effects on urban cellular networks,” *IEEE Trans. Wireless Commun.*, vol. 13, no. 9, pp. 5070–5083, 2014.
- [31] Q. Zhang, W. Saad, M. Bennis, X. Lu, M. Debbah, and W. Zuo, “Predictive deployment of UAV base stations in wireless networks: Machine learning meets contract theory,” *IEEE Trans. Wireless Commun.*, vol. 20, no. 1, pp. 637–652, Jan. 2021.
- [32] R. Courant, F. John, A. A. Blank, and A. Solomon, *Introduction to Calculus and Analysis*. Springer, 1965, vol. 1.
- [33] S. Purkayastha, “Simple proofs of two results on convolutions of unimodal distributions,” *Stat. Probab. Lett.*, vol. 39, no. 2, pp. 97–100, 1998.